

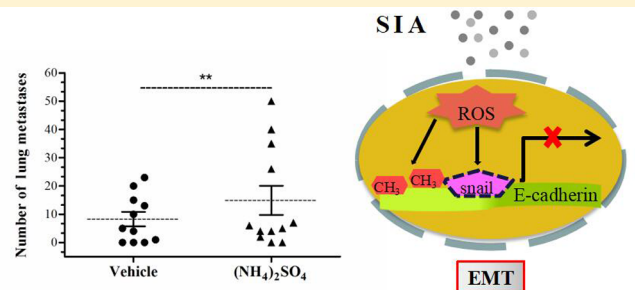
## Sulfate Aerosols Promote Lung Cancer Metastasis by Epigenetically Regulating the Epithelial-to-Mesenchymal Transition (EMT)

Yang Yun, Rui Gao,<sup>†</sup> Huifeng Yue, Lin Guo, Guangke Li, and Nan Sang<sup>\*ID</sup>

College of Environment and Resource, Research Center of Environment and Health, Shanxi University, Taiyuan, Shanxi 030006, P.R. China

### Supporting Information

**ABSTRACT:** Secondary inorganic aerosols (SIA), particularly sulfate aerosols, are central particulate matter (PM) constituents of severe haze formation in China and exert profound impacts on human health; however, our understanding of the mechanisms by which sulfate aerosols cause malignancy in lung carcinogenesis remains incomplete. Here, we show that exposure to secondary inorganic aerosols induced the invasion and migration of lung epithelial cells, and that  $(\text{NH}_4)_2\text{SO}_4$  exerted the most serious effects in vitro and promoted lung tumor metastasis in vivo. This action was associated with alterations of phenotype markers in the epithelial-to-mesenchymal transition (EMT), such as the up-regulation of fibronectin (Fn1) and the down-regulation of E-cadherin (E-cad). Hypoxia-inducible factor 1 $\alpha$  (HIF-1 $\alpha$ )-Snail signaling, regulated by the generation of reactive oxygen species (ROS), was involved in the  $(\text{NH}_4)_2\text{SO}_4$ -induced EMT, and the potent antioxidant N-acetylcysteine (NAC) inhibited the activation of HIF-1 $\alpha$ -Snail and blocked the EMT, cell invasion, and migration in response to  $(\text{NH}_4)_2\text{SO}_4$ . Additionally, CpG hypermethylation in the E-cad promoter regions partly contributed to the  $(\text{NH}_4)_2\text{SO}_4$ -regulated E-cad repression, and the DNA methyltransferase inhibitor 5-aza-2'-deoxycytidine (5-Aza) restored the  $(\text{NH}_4)_2\text{SO}_4$ -induced down-regulation of E-cad. Our findings reveal a potential mechanistic basis for exploring the association between sulfate aerosol exposure and increased malignancy during lung carcinogenesis, and suggest new approaches for the treatment, improvement, and prevention of lung cancer resulting from sulfate aerosol exposure in severe haze-fog.



### INTRODUCTION

Due to the increasing development of industry and the expansion of cities, haze-fog has increased worldwide, particularly in China, and has become the most acute air pollution problem. Recently, China has faced extremely severe and persistent haze pollution, affecting 1.43 million km<sup>2</sup> and 1.1 billion people.<sup>1</sup> With the increasing haze-fog pollution in China, lung cancer mortality has increased by 464.84% during the past three decades.<sup>2</sup> The characteristic features of the winter haze in northern China include low mixing heights, a high relative humidity, high emissions of primary air pollutants, and rapid production of secondary inorganic aerosols, particularly sulfates.<sup>3</sup> Sulfate (SO<sub>4</sub><sup>2-</sup>) is ubiquitous and is a key particulate matter (PM) constituent in the atmosphere.<sup>4</sup> By analyzing the main PM<sub>2.5</sub> species in Xi'an, the SO<sub>4</sub><sup>2-</sup> mass fraction was shown to increase during transition and polluted (hazy) periods; however, there was a slight decrease in the organic matter mass fraction.<sup>4</sup> Many epidemiological studies have shown that severe haze-fog has increased the incidence of lethal diseases, particularly lung cancer.<sup>5,6</sup> During severe haze-fog, whether the high levels of sulfate aerosols promoting lung cancer development has thus attracted increasing public attention.

The epithelial-to-mesenchymal transition (EMT) has been demonstrated to be a critical step in the metastasis of lung

cancer.<sup>7</sup> The processes of the EMT in cancer pathogenesis include the loss of epithelial markers, e.g., E-cadherin (E-cad), and the induction of mesenchymal markers, e.g., fibronectin (Fn1), which is accompanied by the progressive acquisition of a motile and invasive phenotype.<sup>8–11</sup> E-cad, which is a cell surface adhesion glycoprotein, plays a critical role in the EMT-mediated tumor progression.<sup>12</sup> Hypoxia-inducible factor 1 $\alpha$  (HIF-1 $\alpha$ ) is a key mediator of cellular adaptation to hypoxia and induces the transcriptional repressors Snail and Slug, which directly inhibit E-cad expression.<sup>8,13</sup> Moreover, DNA promoter CpG hypermethylation is currently recognized as an important epigenetic event that results in the loss of E-cad function during lung cancer progression.<sup>14</sup> DNA methyltransferase 1 (dnmt-1) induces significant hypermethylation of gene promoters during tumor development.<sup>15,16</sup> Various mechanisms are involved in the loss of E-cad expression during tumor progression.

In polluted environments, the SO<sub>2</sub> oxidation process leads to high sulfate production rates of aqueous particles, which exacerbate the development of persistent severe haze in China.

Received: June 4, 2017

Revised: August 16, 2017

Accepted: August 28, 2017

Reactive oxygen species (ROS) have been reported to be important signaling molecules in cytotoxic reactions directly induced by inhaled SO<sub>2</sub>.<sup>17,18</sup> ROS act as mediators and can contribute to pro-apoptotic actions in lung cancer cells.<sup>19</sup> Additionally, SO<sub>2</sub> induces the formation of ROS and ultimately results in the apoptosis of lung cancer cells.<sup>17</sup> However, the elucidation of the mechanisms by which secondary inorganic aerosols (SIA), particularly sulfate aerosols, contribute to malignancy during lung carcinogenesis in severe haze-fog remains challenging. In this work, we treated human bronchial epithelial cells and a lung metastasis mouse model with (NH<sub>4</sub>)<sub>2</sub>SO<sub>4</sub> and demonstrated that (NH<sub>4</sub>)<sub>2</sub>SO<sub>4</sub> might be associated with the EMT activation. Moreover, we found that the ROS generation mediated-aberrant methylation of the E-cad promoter contributed to the inhibition of E-cad following the (NH<sub>4</sub>)<sub>2</sub>SO<sub>4</sub> exposure.

## MATERIALS AND METHODS

**Cell Culture and Treatment.** Human nonsmall cell lung cancer A549 cells and human bronchial epithelial cells (BEAS-2B) were obtained from the Cell Bank of Type Culture Collection of the Chinese Academy (CAS, China). These cells were cultured in RPMI 1640 medium supplemented with 10% fetal bovine serum (FBS; Gibco, U.S.A.), 100 U/mL penicillin (Gibco, U.S.A.), and 100 U/mL streptomycin (Gibco, U.S.A.). The cells were kept in an incubator under 5% CO<sub>2</sub> and 95% humidity at 37 °C. Before the experiments, the cells were randomly seeded and divided into different groups. The different groups of cells were exposed to various concentrations of NO<sub>3</sub><sup>-</sup> or SO<sub>4</sub><sup>2-</sup> (i.e., 0, 10, 30, 100, and 300 μM) for specific durations (0.5, 1, 3, 6, 12, 24, and 48 h). For the ROS and DNA methyltransferase interference experiment, 1 mM N-acetyl-L-cysteine (NAC; Sigma, U.S.A.) and 5 μM 5-aza-2'-deoxycytidine (5-Aza; Sigma, U.S.A.) were added to the cells 1 h prior to the treatment. For different cell studies, three to six independent experiments for each treatment were conducted in triplicate.

**Nude Mouse Lung Cancer Model.** In total, 30 BALB/c nu/nu mice (6 weeks old) were maintained in a barrier-free animal facility, and A549-Luc cells ( $2 \times 10^5$  cells per mouse) were intravenously injected into the tail vein of each mouse. Then, the mice were divided into the vehicle group and the treatment group (15 mice per group). The mice in the treatment group received an oropharyngeal aspiration administration of (NH<sub>4</sub>)<sub>2</sub>SO<sub>4</sub> (10 mg/kg) every day for 6 weeks, while the vehicle group was treated with sterile saline. The number of nodules reflecting metastasis of A549-Luc were counted using Cri Maestro in vivo imaging systems after two, three, four, five, and six weeks of treatment. Finally, the mice were sacrificed, and the lungs were removed and fixed in 4% paraformaldehyde for further analysis.

**Cell Migration and Invasion Assays.** Before the invasion assay, the cells ( $5 \times 10^5$  cells per mL) were seeded onto 35 mm dishes and treated with different concentrations of NO<sub>3</sub><sup>-</sup> or SO<sub>4</sub><sup>2-</sup> (0, 10, 30, 100, and 300 μM). After different treatment for 48 h, the cells were harvested and seeded in the upper chambers of 24-well plates with serum-free RPMI 1640 (approximately  $2 \times 10^4$  cells per chamber). The lower compartments of the plates were filled with RPMI 1640 containing 10% FBS. After 24 h of incubation, the cells on the upper surface of the chambers were removed, and those that had migrated to the lower surface were fixed with 4% paraformaldehyde and stained with crystal violet. The migrated

cells were randomly photographed under light microscopy (Olympus, Japan) at a magnification of 400×, and five picture fields were quantified for the analysis. There were three repeat transwell inserts for each treatment group, and the assay repeated three times. In this assay, the transwell inserts (8.0 μm pore size) were coated with Matrigel (1.25 mg/mL; BD Biosciences) prior to use.<sup>20</sup>

## Real-time Quantitative Reverse Transcription-PCR.

A549 cells ( $5 \times 10^5$  cells per mL) were seeded onto 35 mm dishes and treated with various concentrations of SO<sub>4</sub><sup>2-</sup> (0, 10, 30, 100, and 300 μM) for 12, 24, and 48 h. The cells were washed twice with PBS and harvested. Total RNA was extracted using the TRIzol Reagent (Invitrogen, U.S.A.) as previously described.<sup>21</sup> First-strand complementary DNA (cDNA) was synthesized using the reverse transcription kit (TaKaRa, China). The real-time PCR amplification was conducted as previously described.<sup>22</sup> The quantification of the gene expression was performed on a qTOWER 2.2 real-time PCR thermal cycler (Analytik Jena AG, Jena, Germany). The relative expression of the gene was calculated using β-actin as an internal control.<sup>23</sup> The primer sequences are listed in Table S1 of the Supporting Information, SI.

**Immunofluorescence.** The cells were treated with various concentrations of SO<sub>4</sub><sup>2-</sup> (0, 30, and 300 μM) for 48 h after seeding on glass slides pretreated with poly-L-lysine (10 μg/mL). The cells were fixed with 4% paraformaldehyde for 15 min and then permeabilized in 0.5% Triton X 100 in PBS for 20 min. After blocking with 5% goat serum for 30 min, the cells were incubated with the anti-E-cad primary antibody (1:200; Bioss; bs-10009R) overnight at 4 °C and the fluorescently labeled goat antirabbit IgG secondary antibody (1:1000, IRDye 800 CW; 926-32211) for 1 h. The cells were counterstained with DAPI before coverslipping in a fluorescence protective agent. The images were captured under a fluorescence microscope (Olympus, Japan) at a magnification of 400×.<sup>24</sup>

Lung tissues fixed in paraformaldehyde were embedded in paraffin and cut into 5-μm sections for the Immunofluorescence analysis of E-cad expression. The experiment was performed according to a routine protocol (SI).

**Western Blot Assays.** A549 and BEAS-2B cells ( $5 \times 10^5$  cells per mL) were seeded onto 35 mm dishes and treated with various concentrations of SO<sub>4</sub><sup>2-</sup> (0, 10, 30, 100, and 300 μM) for 48 h. The cells were washed twice with PBS and harvested by scraping in ice-cold lysis buffer. The supernatants were collected after centrifugation at 13 000 rpm for 15 min. The protein concentration was determined using NanoDrop 2000C (Thermo, China) to ensure the equal loading of samples prior to resolution by sodium dodecyl sulfate (SDS)-polyacrylamide gel electrophoresis (PAGE). After transferring the protein bands to a nitrocellulose membrane, the membrane was blocked with 5% nonfat milk and incubated overnight at 4 °C with primary antibodies against the targeted proteins (anti-β-actin antibody, CST, 4970s; anti-E-cad antibody, Bioss, bs-10009R; anti-NOX1 antibody, Bioss, bs-3682R; anti-SOD2 antibody, Bioss, bs-1080R; anti-GPX1 antibody, Bioss, bs-3882R; anticatalase antibody, Bioss, bs-6874R; anti-Snail-1 antibody, Bioss, bs-1371R; and anti-Dnmt-1 antibody, Bioss, bs-0687R). Then, the membrane was exposed to the fluorescently labeled secondary antibody (1:5000) (IRDye 800 CW goat antirabbit IgG, 926-32211), and the proteins of interest were detected and scanned using the LI-COR Odyssey infrared fluorescent system.

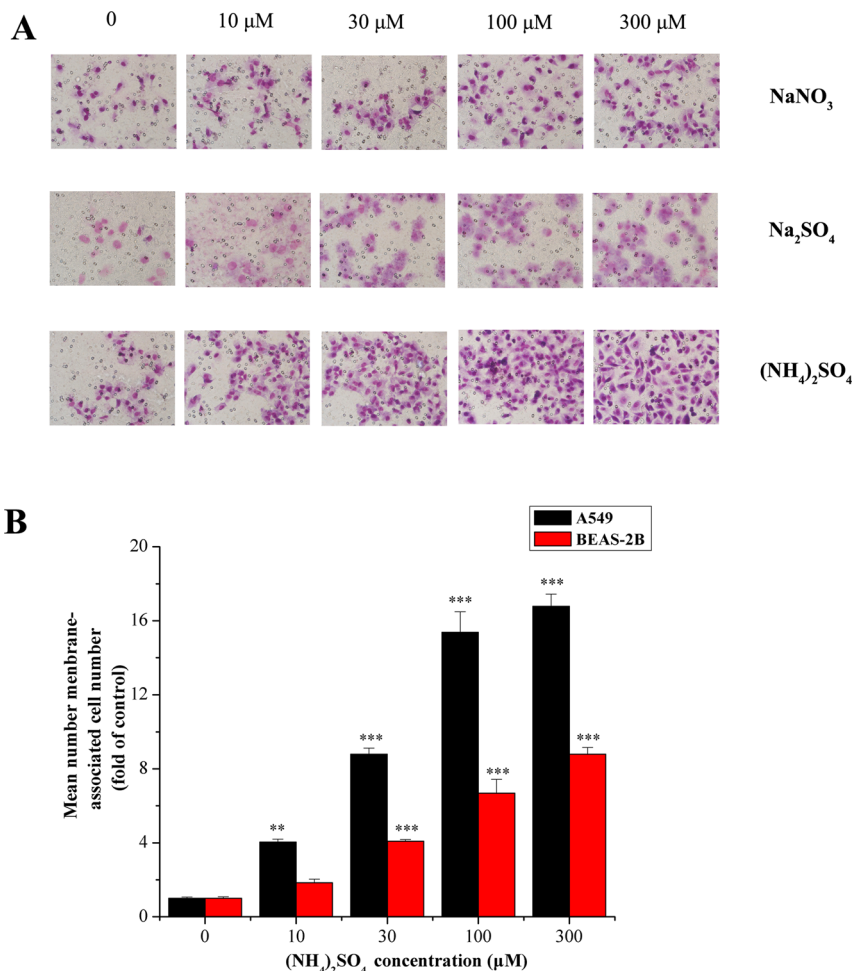


**Figure 1.** SIA induce the invasion and migration of lung epithelial cells. (A) A549 cells were incubated with various concentrations of SIA ( $\text{NO}_3^-$  or  $\text{SO}_4^{2-}$ ) (0, 10, 30, 100, and 300  $\mu\text{M}$ ) for 48 h. The invasive ability was evaluated by the cell invasion assay (400 $\times$ ). (B) A549 cells and BEAS-2B cells were both exposed to various concentrations of  $(\text{NH}_4)_2\text{SO}_4$ , and the migration rates were calculated. \*\* $p < 0.01$  and \*\*\* $p < 0.001$  compared with the control group.

**ROS Detection.** A549 cells ( $5 \times 10^5$  cells per mL) were seeded onto 35 mm dishes and treated with various concentrations of  $\text{SO}_4^{2-}$  (0, 10, 30, 100, and 300  $\mu\text{M}$ ) for 0.5, 1, 3, 6, 12, and 24 h. The cells were incubated with 2',7'-dichlorofluorescein-diacetate (DCFH-DA, 10  $\mu\text{M}$ ) at 37 °C for 30 min in the dark. The formation of the fluorescent oxidized derivative of 2',7'-dichlorofluorescein (DCF) was monitored by flow cytometry (C6, BD, U.S.A.) at an excitation wavelength of 488 nm and emission wavelength of 530 nm. The ROS generation was quantified based on the fluorescence intensity of the fluorescent compound DCF formed by 10 000 cells.<sup>17</sup>

**JC-1 Detection.** After a 1 h incubation with NAC, the A549 cells ( $5 \times 10^5$  cells per mL) were seeded onto 35 mm dishes and treated with 300  $\mu\text{M}$   $\text{SO}_4^{2-}$  for 24 h. The cells were incubated with JC-1 fluorescent dye (1.25  $\mu\text{g}/\text{mL}$ , Beyotime) at 37 °C for 30 min in the dark. After washing the cells with PBS twice, the JC-1 monomer was detected at an excitation wavelength of 514 nm and emission wavelength of 529 nm. The JC-1 aggregates were detected at an excitation wavelength of 585 nm and emission wavelength of 590 nm. The results are expressed as the ratio of JC-1 monomer/JC-1 aggregates.

**Chromatin Immunoprecipitation (CHIP).** A549 cells ( $5 \times 10^5$  cells per mL) were seeded onto 100 mm dishes and treated with 300  $\mu\text{M}$   $\text{SO}_4^{2-}$ . The experiment was conducted

according to the instructions of the Chromatin Immunoprecipitation Assay Kit (Millipore, U.S.A.). In brief, after 24 h of incubation, the cells were fixed with formaldehyde and washed twice with PBS containing protease inhibitors. After scraping the cells in PBS containing protease inhibitors, the cells were pelleted, resuspended in SDS lysis buffer, and sonicated to break the DNA. The samples were centrifuged, and the supernatant was diluted with the ChIP dilution buffer. The samples were precleared to reduce nonspecific background and incubated with the primary antibody (Snail-1, Cell Signaling, 3879) overnight. A salmon sperm DNA/protein A agarose slurry was added to collect the antibody/histone complex. After washing with a different washing buffer, the histone complex was eluted from the antibody, and the histone-DNA cross-link was reversed with NaCl. Finally, DNA was recovered by phenol/chloroform extraction and ethanol precipitation. The PCR reaction and DNA agarose electrophoresis were then conducted.

**Bisulfite Sequencing Analysis (BSP).** A549 cells ( $5 \times 10^5$  cells per mL) were seeded onto 100 mm dishes and treated with various concentrations of  $\text{SO}_4^{2-}$  (0, 30, and 300  $\mu\text{M}$ ). Total DNA was extracted as the instruction of EZgeneTM Tissue gDNA Miniprep Kit (Biomiga, GD2211). BSP of E-cad in A549 cells was conducted in collaboration with Beijing

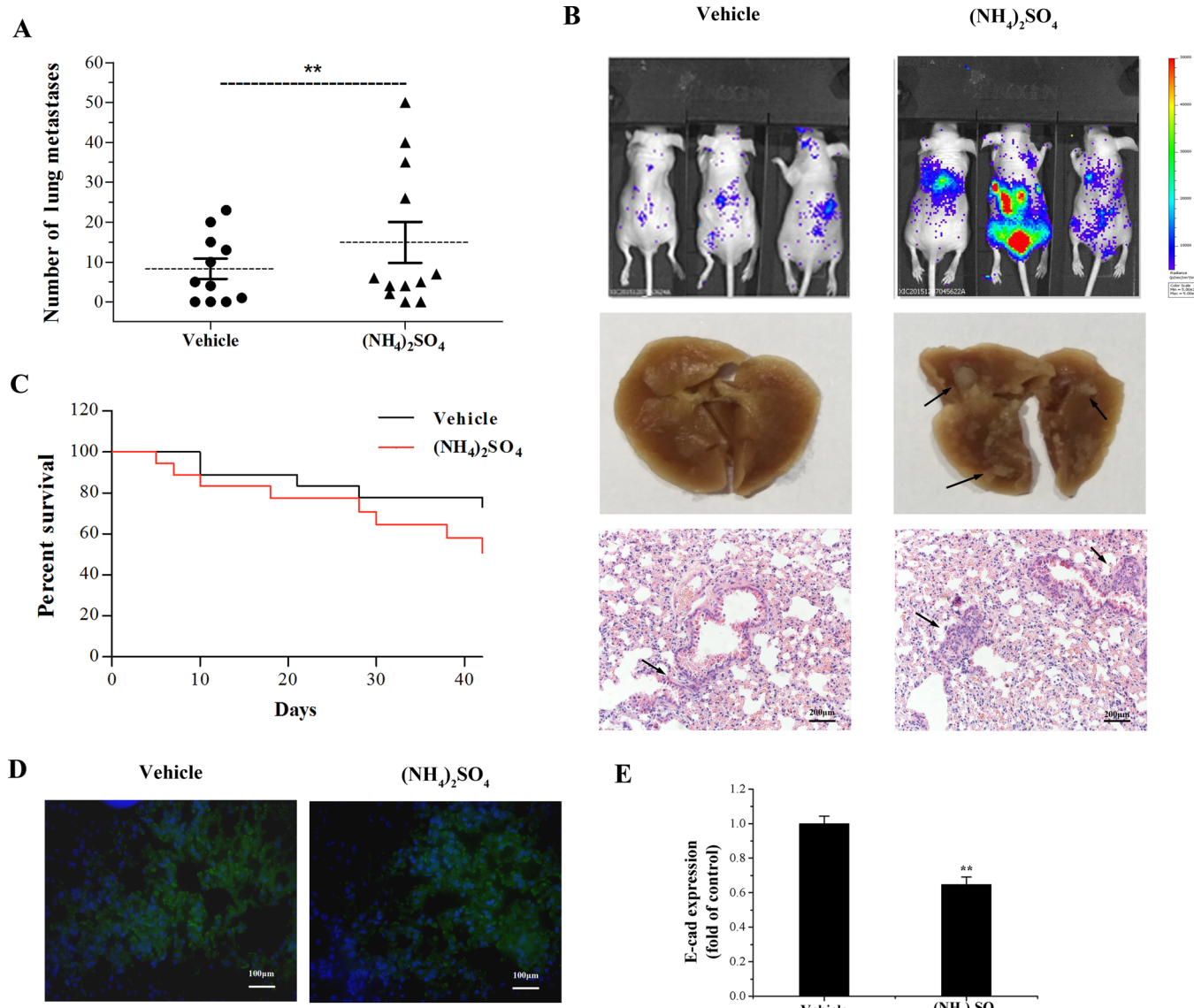


**Figure 2.** (NH<sub>4</sub>)<sub>2</sub>SO<sub>4</sub> exposure promotes lung tumor metastasis in vivo. The effects of (NH<sub>4</sub>)<sub>2</sub>SO<sub>4</sub> exposure on tumor metastases in mice intravenously injected into the tail vein with A549 lung cancer cells expressing Luc (A549-Luc) were examined. (A) The scatter diagrams show the number of nodules representing pulmonary metastases in the vehicle group and treatment group. (B) Representative Luc images of mice, bright-field imaging, and H&E staining of lungs are shown. Arrows indicate the visible nodules. (C) Animal survival was determined using Kaplan–Meier analysis and the log-rank test for data obtained 42 days after building the tumor-burdened model ( $n = 15$ ). (D) The expression of E-cad in lung was detected via immunofluorescence analysis, and the inhibition of E-cad was significantly observed at the exposure group. These values are recorded as the mean  $\pm$  SE  $^{**}p < 0.01$  compared with vehicle group.

Micread Genetics Co., Ltd. Three individual clones from 3 samples and a total of 9 clones from the 0, 30, and 300  $\mu\text{M}$  (NH<sub>4</sub>)<sub>2</sub>SO<sub>4</sub> treatment groups were sequenced.

**Hematoxylin and Eosin (H&E) Staining.** Lung tissues fixed in paraformaldehyde were embedded in paraffin and cut into 5- $\mu\text{m}$  sections. Then, the sections were deparaffinized with xylene, stained with hematoxylin and eosin, and observed by microscopy (Olympus, Japan).

**Statistical Analyses.** The data were analyzed using SPSS version 17.0 software, and the results are presented as the mean  $\pm$  SE. The significance of the differences was determined by one-way ANOVA, followed by Fisher's least significant difference (LSD) test.  $p < 0.05$  was considered statistically significant.

## RESULTS AND DISCUSSION

**Secondary Inorganic Aerosols Induce the Invasion and Migration of Lung Epithelial Cells.** To determine whether the water-soluble inorganic species in PM<sub>2.5</sub> during haze episodes induce the migration of lung cancer cells in lung carcinogenesis and fibrosis, we analyzed the effects of Na<sub>2</sub>SO<sub>4</sub>, NaNO<sub>3</sub>, and (NH<sub>4</sub>)<sub>2</sub>SO<sub>4</sub> on migration using the transwell assays in A549 cells. SO<sub>4</sub><sup>2-</sup>, NO<sub>3</sub><sup>-</sup>, and NH<sub>4</sub><sup>+</sup> represent the dominant anions and cations in fine PM.<sup>4</sup> The migration rates were 1.85-, 4.09-, 6.68-, and 8.79-fold of control after exposure to 10, 30, 100, and 300  $\mu\text{M}$  Na<sub>2</sub>SO<sub>4</sub> for 48 h, respectively. The migration rates only increased by 1.45-, 1.69-, 2.48-, and 2.94-fold of control after exposure to NaNO<sub>3</sub> at the same concentrations. In contrast, the migration rates robustly increased to 4.04-, 8.79-, 15.38-, and 16.79-fold of control

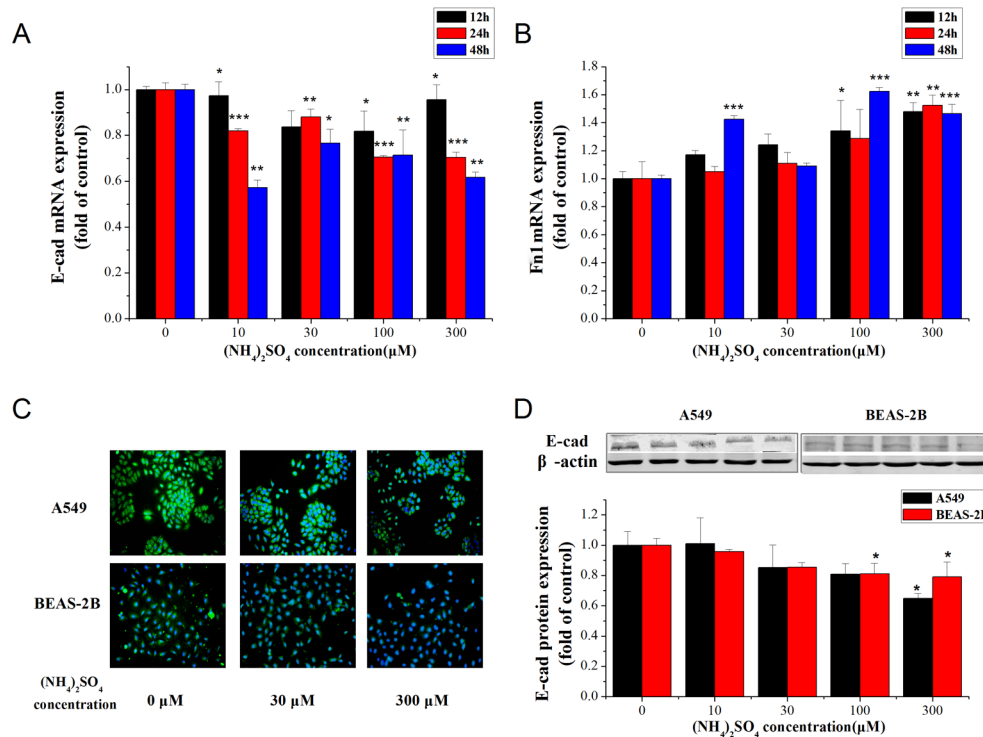


**Figure 3.**  $(\text{NH}_4)_2\text{SO}_4$  induces a concentration- and time-dependent EMT in lung epithelial cells. (A and B) The mRNA expression of E-cad and Fn1 was measured after exposure to different concentrations of  $(\text{NH}_4)_2\text{SO}_4$  for various times (12, 24, and 48 h). (C) Immunofluorescence assays were used to detect the E-cad expression in A549 and BEAS-2B cells after treatment with different concentrations of  $(\text{NH}_4)_2\text{SO}_4$ . (D) The protein expressions of E-cad in A549 and BEAS-2B cells were measured after exposure to different concentrations of  $(\text{NH}_4)_2\text{SO}_4$ . These values are presented as the mean  $\pm$  SE \* $p$  < 0.05, \*\* $p$  < 0.01, and \*\*\* $p$  < 0.001 compared with the control group.

following  $(\text{NH}_4)_2\text{SO}_4$  treatment at the same concentrations (Figure 1A). In addition, to determine whether  $(\text{NH}_4)_2\text{SO}_4$  promotes the invasion and migration process in a lung epithelial cell line, A549 and BEAS-2B cells were both used, and the migration rates were calculated. As shown in Figure 1B, the number of A549 cells that migrated to the membrane was significant higher than that of migrated BEAS-2B cells. These results further support the role of  $(\text{NH}_4)_2\text{SO}_4$  in promoting lung epithelial cell migration, particularly in lung cancer cells.

We quantified the numbers of migrated lung cancer cells after the exposure to  $\text{Na}_2\text{SO}_4$ ,  $\text{NaNO}_3$ , and  $(\text{NH}_4)_2\text{SO}_4$ . Notably, the migration of the lung cancer cells after the exposure to sulfate was larger than that following the exposure to nitrate. This finding was consistent with other studies, such as the Harvard Six Cities Study<sup>25</sup> and the American Cancer Society Study on Particulate Air Pollution and Mortality (ACS study),<sup>26</sup> in which statistically significant associations were found between the sulfate particles and lung cancer mortality.<sup>27,28</sup> In addition, the  $\text{SO}_4^{2-}$  mass fraction increased during transition and polluted (hazy) periods.<sup>4</sup> Hence, sulfate aerosol might be one of important constituents during hazy periods as a risk factor for the development of lung cancer. Because of the presence of high levels of gaseous ammonia (17–23 parts per billion, ppb) during hazy periods,  $\text{SO}_4^{2-}$  and  $\text{NO}_3^-$  in fine PM are completely neutralized.<sup>4</sup> The migration rates after the exposure to  $(\text{NH}_4)_2\text{SO}_4$  were also robustly elevated. Our results indicate that the association between sulfate aerosols during persistent severe haze in China and lung cancer metastasis can be attributed to various components, and  $(\text{NH}_4)_2\text{SO}_4$  plays an important role. To better understand the contribution of sulfate

aerosols in the invasion and migration of lung epithelial cells, we analyzed  $(\text{NH}_4)_2\text{SO}_4$  in subsequent validation experiments.

**$(\text{NH}_4)_2\text{SO}_4$  Exposure Promotes Lung Tumor Metastasis in Vivo.** To determine whether  $(\text{NH}_4)_2\text{SO}_4$  exposure induces tumor cell metastasis in vivo, we examined the effect of the  $(\text{NH}_4)_2\text{SO}_4$  exposure on tumor metastases in mice that were intravenously injected with A549-Luc cells. Compared with the vehicle group,  $(\text{NH}_4)_2\text{SO}_4$  significantly promoted numerous hematogenous metastases of A549-Luc cells in the lung and soft tissues in a time-dependent manner (Figure S1), and the most obvious effect was observed after 42 days of treatment (Figure 2A, B). In addition,  $(\text{NH}_4)_2\text{SO}_4$  reduced the survival rates of the mice in the experimental models (Figure 2C). Then, the expression of E-cad in the lung was detected by an immunofluorescence analysis, and the inhibition of E-cad was significantly observed in the exposure group (Figure 2D, E). These results validate that the tumor cell migration effect of  $(\text{NH}_4)_2\text{SO}_4$  exposure promotes lung tumor metastasis in vivo, and the action was likely associated with the EMT regulation.

**$(\text{NH}_4)_2\text{SO}_4$  Induces a Concentration- and Time-Dependent EMT in Lung Epithelial Cells.** The activation of the EMT is a significant process in cancer cell migration. A decrease in E-cad implies that the epithelial cells lost their cell polarity and cell–cell adhesions, while an increase in Fn1 indicates that the mesenchymal cells acquired migratory and invasive properties.<sup>29,30</sup> In the current study, the mRNA expression of E-cad was significantly decreased upon exposure to low concentrations of  $(\text{NH}_4)_2\text{SO}_4$  for various times (12, 24, and 48 h) (Figure 3A). To better understand the role of  $(\text{NH}_4)_2\text{SO}_4$  in the EMT process, we assessed the transcriptional alteration of Fn1 as another marker of the EMT. In

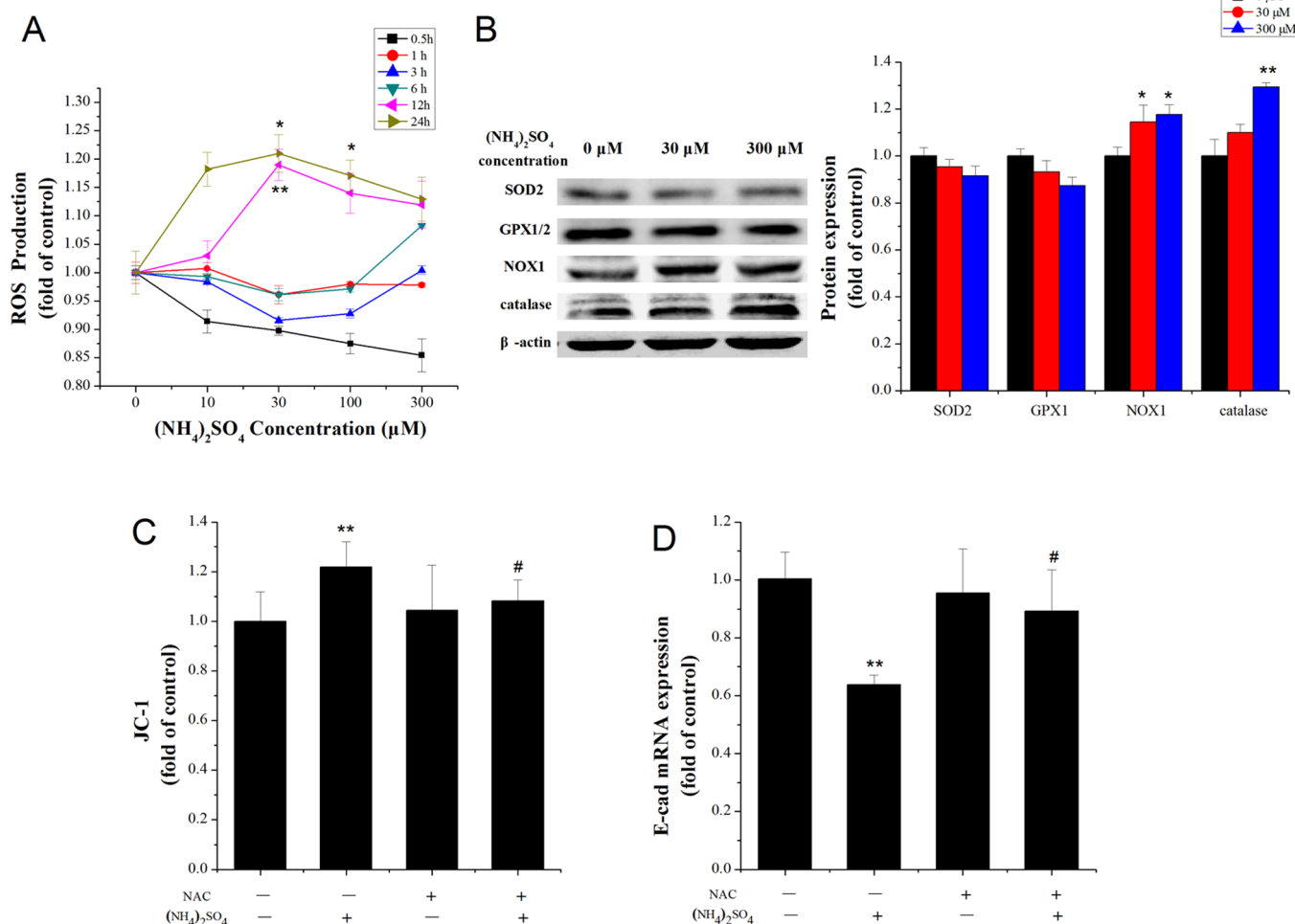


**Figure 4.** ROS generation participates in the  $(\text{NH}_4)_2\text{SO}_4$ -induced EMT in A549 cells. (A) The ROS contents were detected after exposure to different concentrations of  $(\text{NH}_4)_2\text{SO}_4$  for various times (0.5, 1, 3, 6, 12, and 24 h). (B) Western blotting was used to determine the levels of antioxidant enzymes after exposure to different concentrations of  $(\text{NH}_4)_2\text{SO}_4$ . (C) Pretreatment of cells with NAC for 1 h robustly blunted the JC-1 changes following the  $(\text{NH}_4)_2\text{SO}_4$  treatment. (D) Treatment with NAC reversed the loss of E-cad mRNA expression after the  $(\text{NH}_4)_2\text{SO}_4$  exposure. These values are presented as the mean  $\pm$  SE \* $p$  < 0.05 and \*\* $p$  < 0.01 compared with the control group. # $p$  < 0.05 compared with the  $(\text{NH}_4)_2\text{SO}_4$  exposure group.

contrast, the mRNA expression of Fn1 was greatly increased in A549 cells treated with different concentrations of  $(\text{NH}_4)_2\text{SO}_4$  for long exposure times (24 and 48 h) (Figure 3B). Further confirming these findings, the reduction in the cellular morphological changes and the protein expression of E-cad after exposure to various concentrations of  $(\text{NH}_4)_2\text{SO}_4$  for 48 h in both the A549 and the BEAS-2B cell lines (Figure 3C, D) were consistent with the results of the cell migration and invasion experiments following the  $(\text{NH}_4)_2\text{SO}_4$  treatment. All changes reveal that long-term exposure to  $(\text{NH}_4)_2\text{SO}_4$  promotes the EMT in lung cancer cells.

The EMT has been considered a key step in the metastasis of lung and other epithelial tumors.<sup>14</sup> Cancer pathogenesis involves the disruption of normal epithelial integrity, a loss of the morphological features of polarized epithelia, and a gain of mesenchymal markers, accompanied by the progressive acquisition of a motile and invasive phenotype. The loss of E-cad expression is an important step during the EMT developmental program in human lung cancer.<sup>9</sup> Our previous study showed that exposure to  $\text{PM}_{2.5}$  and  $\text{PM}_{10}$  resulted in an EMT activation and extracellular matrix (ECM) degradation in A549 cells.<sup>31</sup> Whereas, as a dominant composition of SIA

during severe haze particulate pollution in north of China, linking these effects specifically to  $(\text{NH}_4)_2\text{SO}_4$ -exposure is somewhat difficult. In this study,  $(\text{NH}_4)_2\text{SO}_4$  resulted in EMT phenotype marker changes, such as a reduction in E-cad and an elevation in Fn1 in both the A549 and the BEAS-2B cell lines. More importantly, we confirmed the above-mentioned results induced by  $(\text{NH}_4)_2\text{SO}_4$  in vivo. In the current study, we established a mouse model of tumor metastasis by inoculating A549-Luc cells into BALB/c nude mice and treating the mice with  $(\text{NH}_4)_2\text{SO}_4$  exposure. Compared with the vehicle group, the  $(\text{NH}_4)_2\text{SO}_4$  exposure caused metastasis of tumor cells and activation of the EMT. These findings suggest that SIA might promote lung cancer metastasis, and this effect was likely a result of driving the EMT developmental program.

**ROS Generation Participates in the  $(\text{NH}_4)_2\text{SO}_4$ -Induced EMT in the A549 Cells.** ROS are important signaling molecules that contribute to the EMT.<sup>32</sup> To investigate whether  $(\text{NH}_4)_2\text{SO}_4$  results in ROS generation, the cells were treated with ROS-sensitive probes and analyzed by flow cytometry. While  $(\text{NH}_4)_2\text{SO}_4$  slightly increased ROS generation after 12 and 24 h, no changes were observed after a short-term (0.5, 1, 3, and 6 h) exposure (Figure 4A). We

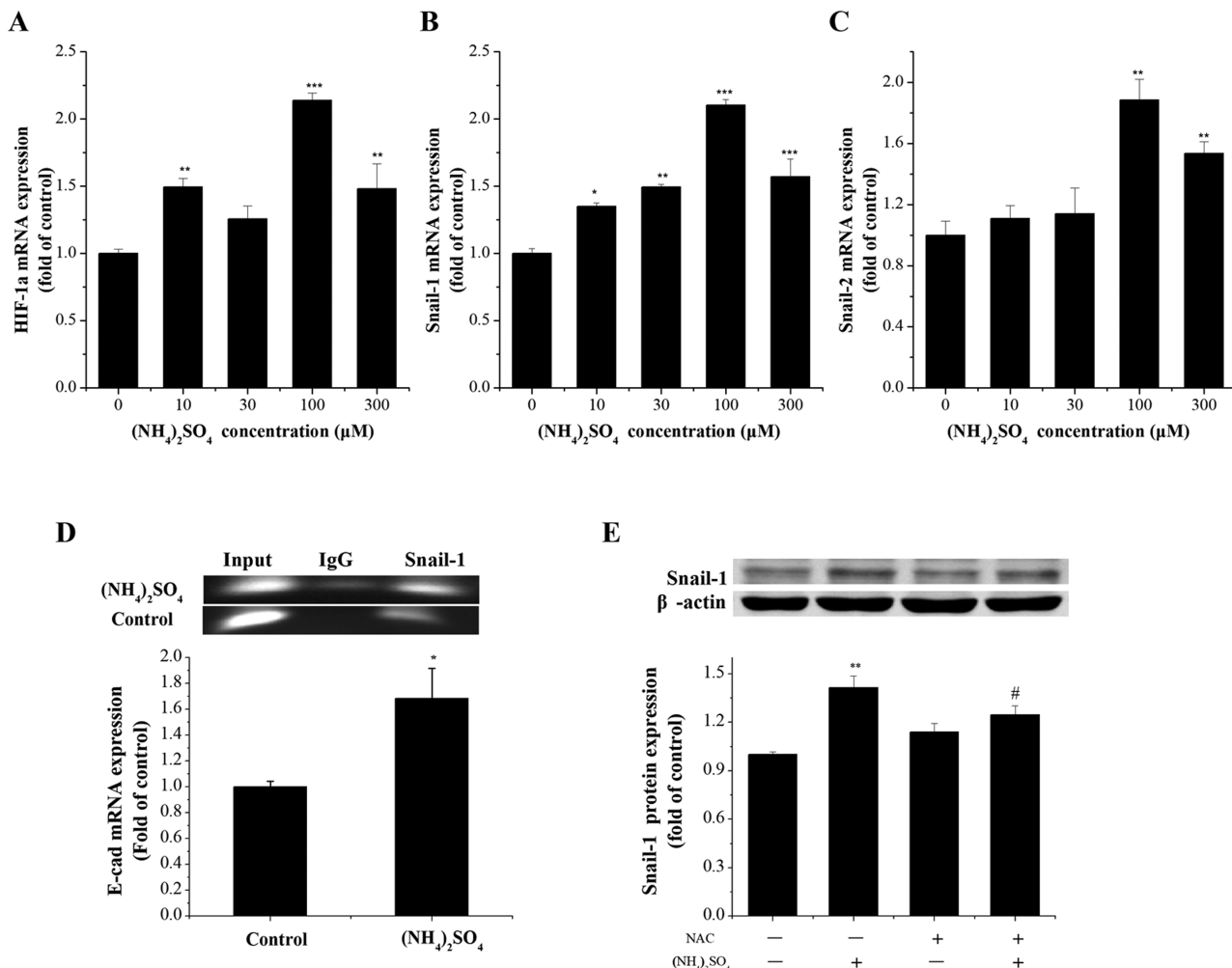


**Figure 5.** HIF-1 $\alpha$  and Snail are involved in the ( $\text{NH}_4\text{}_2\text{SO}_4$ ) inhibition of E-cad expression. (A–C) The mRNA levels of HIF-1 $\alpha$ , Snail-1, and Snail-2 were determined in A549 cells after exposure to ( $\text{NH}_4\text{}_2\text{SO}_4$ ) by qRT-PCR analyses. (D) The efficient binding of the Snail-1 and E-cad promoters was assessed by the ChIP assay after exposure to 300  $\mu\text{M}$  ( $\text{NH}_4\text{}_2\text{SO}_4$ ). (E) After the NAC pretreatment, the expression of the Snail-1 protein was suppressed efficiently. These values are presented as the mean  $\pm$  SE \* $p$  < 0.05, \*\* $p$  < 0.01, and \*\*\* $p$  < 0.001 compared with the control group. # $p$  < 0.05 compared with the ( $\text{NH}_4\text{}_2\text{SO}_4$ ) exposure group.

further determined the effects of antioxidant enzymes following the ( $\text{NH}_4\text{}_2\text{SO}_4$ ) treatment. NOX1 and catalase were slightly increased, whereas SOD2 and GPX1 were reduced with increasing concentrations of ( $\text{NH}_4\text{}_2\text{SO}_4$ ) (Figure 4B). Then, we assessed the mitochondrial membrane potential alterations after the ( $\text{NH}_4\text{}_2\text{SO}_4$ ) exposure. ( $\text{NH}_4\text{}_2\text{SO}_4$ ) treatment increased JC-1, and pretreatment of the cells with NAC for 1 h robustly blunted the JC-1 change following the ( $\text{NH}_4\text{}_2\text{SO}_4$ ) treatment (Figure 4C). In addition, NAC reversed the loss of E-cad expression after the ( $\text{NH}_4\text{}_2\text{SO}_4$ ) exposure (Figure 4D). These results indicate that the mitochondrial dysfunction results in ROS production, which contributes to the ( $\text{NH}_4\text{}_2\text{SO}_4$ )-induced EMT.

ROS are key signaling molecules that contribute to the inhaled  $\text{SO}_2$ -induced cytotoxic reactions.<sup>33,34</sup> In addition, ROS generation is an important contributor to the EMT progression and tumor metastasis.<sup>32</sup> Notably, the slight alteration in ROS generation by the ( $\text{NH}_4\text{}_2\text{SO}_4$ ) stimulation is likely due to the instability of the superoxide anion, and ROS rapidly dismutate in response to  $\text{H}_2\text{O}_2$ .<sup>32</sup> In our study, although there were no apparent concentration and time effects following the ( $\text{NH}_4\text{}_2\text{SO}_4$ ) treatment, the ROS generation after the

( $\text{NH}_4\text{}_2\text{SO}_4$ ) stimulation repressed the expression of E-cad. Thus, prolonged ROS stress was potentially implicated in the progression of carcinogenesis following ( $\text{NH}_4\text{}_2\text{SO}_4$ ) exposure. The balance between ROS production and antioxidant defense determines the degree of oxidative stress.<sup>35</sup> In the current study, the expression of NOX1 and catalase increased, while that of SOD2 and GPX1 decreased after the ( $\text{NH}_4\text{}_2\text{SO}_4$ ) treatment, which further confirm that the superoxide anion partly associated with the ( $\text{NH}_4\text{}_2\text{SO}_4$ ) stimulation induced the EMT. Therefore,  $\text{H}_2\text{O}_2$  following the ( $\text{NH}_4\text{}_2\text{SO}_4$ ) exposure might be obtained through different pathways. JC-1 represents a measurement of mitochondrial depolarization as an early marker of cell apoptosis.<sup>32</sup> NAC eliminated the mitochondrial depolarization and restored the expression of E-cad following the ( $\text{NH}_4\text{}_2\text{SO}_4$ ) exposure, indicating that ROS antioxidants may be beneficial in lung cancer metastasis.

**HIF-1 $\alpha$  and Snail are Involved in the ( $\text{NH}_4\text{}_2\text{SO}_4$ )-Inhibited E-cad Expression.** HIF-1 $\alpha$ , which is induced in hypoxic tumor microenvironments, plays a critical role in adapting the cellular response to oxygen stress.<sup>36</sup> HIF-1 $\alpha$  has been reported to regulate the transcription of multiple genes in tumor cells, and elevated HIF-1 $\alpha$  expression is associated with

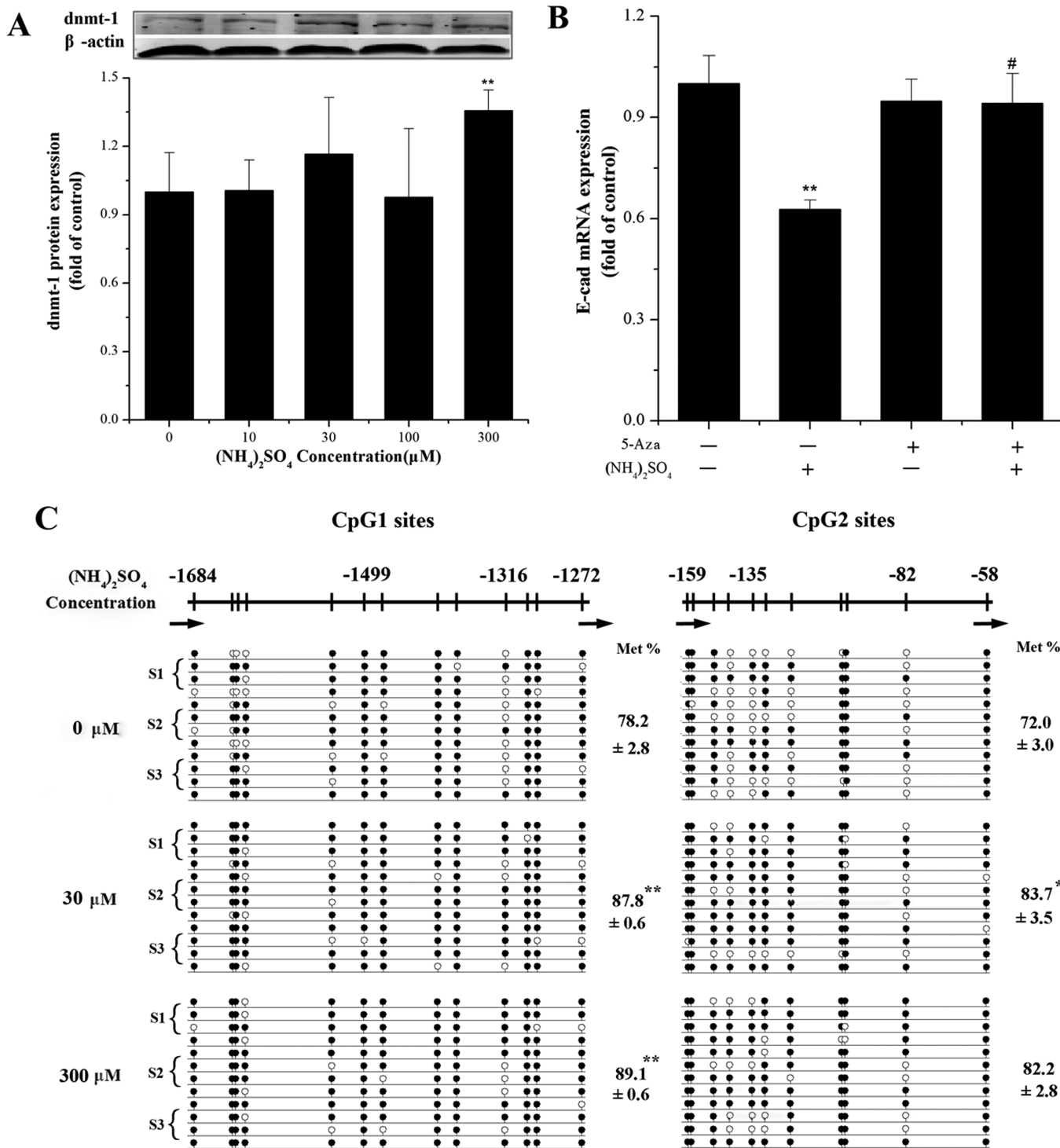


**Figure 6.** Hypermethylation of the E-cad promoter regions partly contributes to the (NH<sub>4</sub>)<sub>2</sub>SO<sub>4</sub> regulation of E-cad repression. (A) Exposure to (NH<sub>4</sub>)<sub>2</sub>SO<sub>4</sub> caused an up-regulation of the dnmt-1 protein expression in A549 cells. (B) Pretreatment with 5-Aza restored the reduced expression of E-cad mRNA after the (NH<sub>4</sub>)<sub>2</sub>SO<sub>4</sub> exposure. (C) BSP was performed to determine the methylation status of the CpG islands at the E-cad promoter after the (NH<sub>4</sub>)<sub>2</sub>SO<sub>4</sub> exposure. These values are presented as the mean  $\pm$  SE \* $p$  < 0.05 and \*\* $p$  < 0.01 compared with the control group. # $p$  < 0.05 compared with the (NH<sub>4</sub>)<sub>2</sub>SO<sub>4</sub> exposure group.

tumor metastasis.<sup>37,38</sup> To determine whether the up-regulation of HIF-1 $\alpha$  plays an important role in the (NH<sub>4</sub>)<sub>2</sub>SO<sub>4</sub>-repressed expression of E-cad, we measured the HIF-1 $\alpha$  expression in A549 cells treated with (NH<sub>4</sub>)<sub>2</sub>SO<sub>4</sub>. As indicated in Figure 5A, the different concentrations of (NH<sub>4</sub>)<sub>2</sub>SO<sub>4</sub> significantly elevated HIF-1 $\alpha$  expression, suggesting that the ROS

production partially stimulates HIF-1 $\alpha$  activation in the (NH<sub>4</sub>)<sub>2</sub>SO<sub>4</sub>-induced tumor metastasis in A549 cells.

Snail, which is a transcription repressor that directly inhibits the transcription of E-cad, is a keystone to the epithelial state in EMT.<sup>39</sup> To clarify the molecular mechanism by which (NH<sub>4</sub>)<sub>2</sub>SO<sub>4</sub> repressed E-cad expression via the regulation of transcriptional factors, we assessed the expression of Snail-1

and Snail-2/Slug in the A549 cells. Compared with the control,  $(\text{NH}_4)_2\text{SO}_4$  increased the expression of Snail-1 and Snail-2. An obvious concentration-effect was observed in the Snail-1 up-regulation (Figure 5B, C), indicating that the binding affinity to the E-cad promoter of Snail-1 is stronger than that of Snail-2. To assess the efficacy of the binding of Snail-1 to the E-cad promoter, a CHIP assay was performed after the exposure to 300  $\mu\text{M}$   $(\text{NH}_4)_2\text{SO}_4$  (Figure 5D). The specific binding of Snail-1 was clearly higher than the nonspecific background binding, indicating that Snail-1 contributes to the  $(\text{NH}_4)_2\text{SO}_4$  induced E-cad repression. We further examined whether the  $(\text{NH}_4)_2\text{SO}_4$  simultaneously induced-ROS production activates the transcriptional repressor of Snail-1. The elevated Snail-1 could bind efficiently to the E-cad promoter, suppress the transcription of E-cad, and ultimately induce the EMT. Alternatively, after the NAC pretreatment, which blocked ROS production, the expression of Snail-1 was suppressed efficiently (Figure 5E).

Hypoxia increases the mitochondrial ROS production, which contributes to the hypoxia-induced EMT.<sup>37,38</sup> Furthermore, accumulated HIF-1 $\alpha$  enhances the transcriptional activity of Snail-1 and Snail-2, which represses the expression of E-cad, thereby promoting the EMT.<sup>40</sup> In our study, we observed the induction of the EMT by the up-regulation of HIF-1 $\alpha$ , Snail-1, and Snail-2 mRNA expression following the treatment with various concentrations of  $(\text{NH}_4)_2\text{SO}_4$ . The CHIP results demonstrated that Snail-1 bound to the E-cad promoter region in the  $(\text{NH}_4)_2\text{SO}_4$ -treated cells, thereby facilitating the suppression of E-cad transcription. Our results are consistent with previous reports in which the stabilization of HIF-1 $\alpha$  directly regulated the EMT, which is required for the hypoxia-induced mitochondrial ROS generation.<sup>41</sup> The initiation of the EMT requires the induction of the E-cad transcriptional repressors Snail-1 and/or Snail-2.<sup>42</sup> Similarly, HIF-1 $\alpha$  acted in cooperation with Snail-1 and Snail-2 and inhibited E-cad expression following exposure to carcinogenic Ni compounds.<sup>32</sup>

**Hypermethylation of E-cad Promoter Regions Partly Contributed to the  $(\text{NH}_4)_2\text{SO}_4$  Regulation of E-cad Repression.** Increasing evidence suggests that the aberrant methylation of the E-cad promoter is involved in the epigenetic mechanisms of transcriptional silencing of the E-cad gene in non-small lung cancer cells.<sup>43,44</sup> Dnmt-1, which is a DNA methyltransferase enzyme that contributes to the maintenance DNA methylation, has been involved in the aberrant promoter methylation of E-cad.<sup>45</sup> Compared with the control group, the  $(\text{NH}_4)_2\text{SO}_4$  exposure caused the up-regulation of dnmt-1 expression (Figure 6A). To confirm whether the  $(\text{NH}_4)_2\text{SO}_4$  induced suppression of E-cad expression is caused by epigenetic regulation, the A549 cells were pretreated with 5-Aza, which is a DNA methyltransferase inhibitor, and E-cad expression was restored following the treatment with  $(\text{NH}_4)_2\text{SO}_4$  (Figure 6B). In addition, BSP was conducted to further explore the methylation status of CpG islands in the E-cad promoter. As shown in Figure 6C, compared to the control group, the methylated CpG sites were more dense in the  $(\text{NH}_4)_2\text{SO}_4$ -treated A549 cells, particularly at CpG sites -1316, -143, -135, and -82. A concentration-dependent promoted trend was also present. These data suggest that  $(\text{NH}_4)_2\text{SO}_4$  represses E-cad expression by the methylation of CpG islands in the E-cad promoter.

The induction of the EMT is epigenetically driven by DNA promoter CpG hypermethylation, histone modifications, and microRNAs.<sup>14</sup> Carcinogen exposure-induced gene promoter hypermethylation is mediated by dnmt-1 in bronchial epithelial

cells.<sup>46</sup> ROS generation induces E-cad promoter hypermethylation through the accumulation of dnmt-1.<sup>47</sup> The present study shows that the  $(\text{NH}_4)_2\text{SO}_4$  exposure significantly elevated dnmt-1 expression at higher concentration and restored E-cad expression following a pretreatment with 5-Aza. Moreover, ROS induces the hypermethylation of the E-cad promoter by elevating Snail expression.<sup>48</sup> Thus, E-cad is repressed by Snail through transcriptional inhibition and the activation of the E-cad promoter hypermethylation in the  $(\text{NH}_4)_2\text{SO}_4$ -induced EMT in A549 cells.

In conclusion, our data provide evidence that  $(\text{NH}_4)_2\text{SO}_4$  exposure might promote the EMT and early lung cancer metastasis. This action was associated with the repression of E-cad by ROS-regulated Snail through transcriptional inhibition and the activation of E-cad promoter hypermethylation. These findings implicate novel insights into tumor development by exploring the association between  $(\text{NH}_4)_2\text{SO}_4$  exposure in a haze-polluted environment and the increased risk of early lung cancer metastasis. We acknowledge that there remain limitations in our study for drawing general conclusions on employed oral administration of supra ambient doses of sulfates. Inhalation of SIA more closely mimics occupational and environmental settings than aspiration in that exposures are to more dispersed SIA structures.<sup>49</sup> Moreover, inhalation administration may avoid potential and artifactual effects on pulmonary response of large mats and agglomerates formed during instillation exposure procedures.<sup>50</sup> Nevertheless, studies by other investigators have confirmed this basic finding that outcomes of inhalation exposure to respirable particles were very similar to those seen after pharyngeal exposure route leading to pulmonary toxicity, and the chain of pathological events was realized through synergized interactions of inflammatory response and oxidative stress culminating in the development of multifocal granulomatous pneumonia, interstitial fibrosis, and mutagenesis.<sup>49</sup> Because of exposure to  $(\text{NH}_4)_2\text{SO}_4$  by aspiration vs inhalation more potent than aspiration of an equivalent mass of SIA in our preliminary experiment, the oropharyngeal aspiration of sulfates was a kind of optimized way of administration in the present study. Another limitation is that we chose  $(\text{NH}_4)_2\text{SO}_4$  exposure level in present in vivo study higher than that in grade II of  $\text{PM}_{2.5}$  in China (0.075 mg/m<sup>3</sup>), but still in the range of reported maximum  $\text{PM}_{2.5}$  levels.  $\text{PM}_{2.5}$  mean mass concentration was under the haze weather of 0.692 mg/m<sup>3</sup> reached in Taiyuan.<sup>51</sup> Although the present experiments may be beyond the normal urban SIA concentration encountered in the human atmosphere environment, the animals were subjected to regular periods of extended exposure (i.e., 10 mg/kg every day for 6 weeks). This may provide a corollary to individuals exposed to SIA in severe haze-fog for long-term year after year. Also considering the complicated components or a component's contribution to carcinogenic toxicity of actual ambient  $\text{PM}_{2.5}$ , we employed oropharyngeal aspiration of supra ambient doses of SIA. Further study is needed for the potential mechanism of actual ambient concentration of SIA promotes lung cancer metastasis.

## ASSOCIATED CONTENT

### Supporting Information

The Supporting Information is available free of charge on the ACS Publications website at DOI: 10.1021/acs.est.7b02857.

Table S1. Primer sequences used for real-time RT-PCR; Figure S1.  $(\text{NH}_4)_2\text{SO}_4$  exposure promotes numerous hematogenous metastases of A549-Luc cells in the lung and soft tissues in a time-dependent manner; and a detailed description of the Immunohistochemistry Method (PDF)

## AUTHOR INFORMATION

### Corresponding Author

\*Tel.: +86-351-7011932; fax: +86-351-7011932; e-mail: sangnan@sxu.edu.cn (N.S.).

### ORCID

Nan Sang: 0000-0002-2433-3200

### Author Contributions

<sup>†</sup>Y.Y. and R.G. contributed equally to this work.

### Notes

The authors declare no competing financial interest.

## ACKNOWLEDGMENTS

This study was supported by National Science Foundation of China (No. 21377076, 91543203, 21677091, 21477070, 21222701), Research Project for Shanxi Young Sanjin Scholarship of China, Program for the Outstanding Innovative Teams of Higher Learning Institutions of Shanxi, Program for the Outstanding Youth Academic Leaders of Higher Learning Institutions of Shanxi, and Research Project Supported by Shanxi Scholarship Council of China (No. 2015-006).

## REFERENCES

- 1) Zheng, G.; Duan, F.; Ma, Y.; Zhang, Q. Episode-Based Evolution Pattern Analysis of Haze Pollution: Method Development and Results from Beijing, China. *Environ. Sci. Technol.* **2016**, *50* (9), 4632–4641.
- 2) She, J.; Yang, P.; Hong, Q.; Bai, C. Lung cancer in China: challenges and interventions. *Chest* **2013**, *143* (4), 1117–1126.
- 3) Cheng, Y.; Zheng, G.; Wei, C.; Mu, Q.; Zheng, B.; Wang, Z.; Gao, M.; Zhang, Q.; He, K.; Carmichael, G.; Pöschl, U.; Su, H. Reactive nitrogen chemistry in aerosol water as a source of sulfate during haze events in China. *Sci. Adv.* **2016**, *2* (12), e1601530.
- 4) Wang, G.; Zhang, R.; Gomez, M. E.; Yang, L.; Zamora, M. L.; Zamora, M.; Hu, M.; Lin, Y.; Peng, J. Persistent sulfate formation from London Fog to Chinese haze. *Proc. Natl. Acad. Sci. U. S. A.* **2016**, *113* (48), 13630–13635.
- 5) Fajersztajn, L.; Veras, M.; Barrozo, L. V.; Saldiva, P. Air pollution: a potentially modifiable risk factor for lung cancer. *Nat. Rev. Cancer* **2013**, *13* (9), 674–678.
- 6) Betha, R.; Behera, S. N.; Balasubramanian, R. 2013 Southeast Asian smoke haze: fractionation of particulate-bound elements and associated health risk. *Environ. Sci. Technol.* **2014**, *48* (8), 4327–4335.
- 7) Guarino, M.; Rubino, B.; Ballabio, G. The role of epithelial-mesenchymal transition in cancer pathology. *Pathology* **2007**, *39*, 305–18.
- 8) Islam, S.; Carey, T. E.; Wolf, G. T.; Wheelock, M. J.; Johnson, K. R. Expression of N-cadherin by human squamous carcinoma cells induces a scattered fibroblastic phenotype with disrupted cell-cell adhesion. *J. Cell Biol.* **1996**, *135* (6), 1643–1654.
- 9) Gibbons, D. L.; Lin, W.; Creighton, C. J.; Rizvi, Z. H.; Gregory, P. A.; Goodall, G. J.; et al. Contextual extracellular cues promote tumor cell EMT and metastasis by regulating miR-200 family expression. *Genes Dev.* **2009**, *23*, 2140–2151.
- 10) Huber, M. A.; Kraut, N.; Beug, H. Molecular requirements for epithelial-mesenchymal transition during tumor progression. *Curr. Opin. Cell Biol.* **2005**, *17* (5), 548–558.
- 11) Dohadwala, M.; Yang, S. C.; Luo, J.; Sharma, S.; Batra, R. K.; Huang, M.; Lin, Y.; Goodlick, L. Cyclooxygenase-2-dependent regulation of E-cadherin: prostaglandin E (2) induces transcriptional repressors ZEB1 and snail in non-small cell lung cancer. *Cancer Res.* **2006**, *66* (10), 5338–5345.
- 12) Chen, J.; Imanaka, N.; Chen, J.; Griffin, J. D. Hypoxia potentiates Notch signaling in breast cancer leading to decreased E-cadherin expression and increased cell migration and invasion. *Br. J. Cancer* **2010**, *102*, 351–360.
- 13) Thiery, J. P.; Sleeman, J. P. Complex networks orchestrate epithelial-mesenchymal transitions. *Nat. Rev. Mol. Cell Biol.* **2006**, *7* (2), 131–142.
- 14) Tellez, C. S.; Juri, D. E.; Do, K.; Bernauer, A. M.; Thomas, C. L.; Damiani, L. A.; Tessema, M.; Leng, S.; Belinsky, S. A. EMT and stem cell-like properties associated with miR-205 and miR-200 epigenetic silencing are early manifestations during carcinogen-induced transformation of human lung epithelial cells. *Cancer Res.* **2011**, *71*, 3087–3097.
- 15) Perry, A. S.; Baird, A. M.; Gray, S. G. Epigenetic Methodologies for the Study of Celiac Disease. *Methods Mol. Biol.* **2015**, *1326*, 131–158.
- 16) Shinjo, K.; Kondo, Y. Targeting cancer epigenetics: Linking basic biology to clinical medicine. *Adv. Drug Delivery Rev.* **2015**, *95*, 56–64.
- 17) Yun, Y.; Gao, R.; Yue, H.; Li, G.; Zhu, N.; Sang, N. Synergistic effects of particulate matter ( $\text{PM}_{10}$ ) and  $\text{SO}_2$  on human non-small cell lung cancer A549 via ROS-mediated NF- $\kappa$ B activation. *J. Environ. Sci. (Beijing, China)* **2015**, *31*, 146–153.
- 18) Wei, A.; Fu, B.; Wang, Y.; Zhai, X.; Xin, X.; Zhang, C.; Cao, D.; Zhang, X. Involvement of NO and ROS in sulfur dioxide induced guard cells apoptosis in *Tagetes erecta*. *Ecotoxicol. Environ. Saf.* **2015**, *114*, 198–203.
- 19) Wang, Y.; Sun, Z.; Chen, S.; Jiao, Y.; Bai, C. ROS-mediated activation of JNK/p38 contributes partially to the pro-apoptotic effect of ajoene on cells of lung adenocarcinoma. *Tumor Biol.* **2016**, *37* (3), 3727–3738.
- 20) Yue, H.; Yun, Y.; Gao, R.; Li, G.; Sang, N. Winter Polycyclic Aromatic Hydrocarbon-Bound Particulate Matter from Peri-urban North China Promotes Lung Cancer Cell Metastasis. *Environ. Sci. Technol.* **2015**, *49* (24), 14484–14493.
- 21) Lan, J.; Gou, N.; Gao, C.; He, M.; Gu, A. Z. Comparative and mechanistic genotoxicity assessment of nanomaterials via a quantitative toxicogenomics approach across multiple species. *Environ. Sci. Technol.* **2014**, *48* (21), 12937–12945.
- 22) Yun, Y.; Li, H.; Li, G.; Sang, N.  $\text{SO}_2$  inhalation modulates the expression of apoptosis-related genes in rat hippocampus via its derivatives in vivo. *Inhalation Toxicol.* **2010**, *22* (11), 919–929.
- 23) Guo, L.; Li, B.; Miao, J.; Yun, Y.; Li, G.; Sang, N. Seasonal variation in air particulate matter ( $\text{PM}_{10}$ ) exposure-induced ischemia-like injuries in the rat brain. *Chem. Res. Toxicol.* **2015**, *28* (3), 431–439.
- 24) Realini, N.; Palese, F.; Pizzirani, D.; Pontis, S.; Basit, A.; Bach, A.; Ganeshan, A.; Piomelli, D. Acid ceramidase in melanoma: expression, localization and effects of pharmacological inhibition. *J. Biol. Chem.* **2016**, *291* (5), 2422–2434.
- 25) Dockery, D. W.; Pope, C. A., III; Xu, X.; Spengler, J. D.; Ware, J. H.; Fay, M. E.; Ferris, B. G., Jr; Speizer, F. E. An association between air pollution and mortality in six U.S. cities. *N. Engl. J. Med.* **1993**, *329* (24), 1753–1759.
- 26) Pope, C. A., III; Thun, M. J.; Namboodiri, M. M.; Dockery, D. W.; Evans, J. S.; Speizer, F. E.; Heath, C. W., Jr Particulate air pollution as a predictor of mortality in a prospective study of U.S. adults. *Am. J. Respir. Crit. Care Med.* **1995**, *151* (3), 669–674.
- 27) Krewski, D.; Burnett, R. T.; Goldberg, M. S.; Hoover, K.; Siemiatycki, J.; Jerrett, M.; Abrahamowicz, M.; White, W. H. Overview of the reanalysis of the Harvard Six Cities Study and the American Cancer Society Study of Particulate Air Pollution and Mortality. *J. Toxicol. Environ. Health, Part A* **2003**, *66* (16–19), 1507–1551.
- 28) Raaschou-Nielsen, O.; Beelen, R.; Wang, M.; Hoek, G.; Andersen, Z. J.; Hoffmann, B.; Stafoggia, M.; Samoli, E.; Weinmayr, G.; Dimakopoulou, K.; et al. Particulate matter air pollution components and risk for lung cancer. *Environ. Int.* **2016**, *87*, 66–73.

- (29) Kalluri, R.; Weinberg, R. A. The basics of epithelial-mesenchymal transition. *J. Clin. Invest.* **2009**, *119*, 1420–1428.
- (30) Rastaldi, M. P.; Ferrario, F.; Giardino, L.; Dell'Antonio, G.; Grillo, C.; Grillo, P.; et al. Epithelial-mesenchymal transition of tubular epithelial cells in human renal biopsies. *Kidney Int.* **2002**, *62* (1), 137–146.
- (31) Yan, W.; Ku, T.; Yue, H.; Li, G.; Sang, N. NO<sub>2</sub> inhalation causes tauopathy by disturbing the insulin signaling pathway. *Chemosphere* **2016**, *165*, 248–256.
- (32) Wu, C. H.; Tang, S. C.; Wang, P. H.; Lee, H.; Ko, J. L. Nickel-induced epithelial-mesenchymal transition by reactive oxygen species generation and E-cadherin promoter hypermethylation. *J. Biol. Chem.* **2012**, *287* (30), 25292–25302.
- (33) Qin, G.; Meng, Z. Effect of sulfur dioxide inhalation on CYP1A1 and CYP1A2 in rat liver and lung. *Toxicol. Lett.* **2005**, *160* (1), 34–42.
- (34) Labbé, P.; Pelletier, M.; Omara, F. O.; Girard, D. Functional responses of human neutrophils to sodium sulfite (Na<sub>2</sub>SO<sub>3</sub>) in vitro. *Hum. Exp. Toxicol.* **1998**, *17* (11), 600–605.
- (35) Finkel, T.; Holbrook, N. J. Oxidants, oxidative stress and the biology of ageing. *Nature* **2000**, *408* (6809), 239–247.
- (36) Vaupel, P. The role of hypoxia-induced factors in tumor progression. *Oncologist* **2004**, *9*, 10–17.
- (37) Ziello, J. E.; Jovin, I. S.; Huang, Y. Hypoxia-Inducible Factor (HIF)-1 regulatory pathway and its potential for therapeutic intervention in malignancy and ischemia. *Yale J. Biol. Med.* **2007**, *80* (2), 51–60.
- (38) Gu, Q.; He, Y.; Ji, J.; Yao, Y.; Shen, W.; Luo, J.; Zhu, W.; Cao, H.; Geng, Y.; Xu, J.; Zhang, S.; Cao, J.; Ding, W. Q. Hypoxia-inducible factor 1α (HIF-1α) and reactive oxygen species (ROS) mediates radiation-induced invasiveness through the SDF-1α/CXCR4 pathway in non-small cell lung carcinoma cells. *Oncotarget* **2015**, *6* (13), 10893–10907.
- (39) Valastyan, S.; Weinberg, R. A. Tumor Metastasis: Molecular Insights and Evolving Paradigms. *Cell* **2011**, *147* (2), 275–292.
- (40) Villarejo, A.; Cortés-Cabrera, A.; Molina-Ortíz, P.; Portillo, F.; Cano, A. Patricia Molina-Ortíz, Francisco Portillo, Amparo Cano. Differential Role of Snail1 and Snail2 Zinc Fingers in E-cadherin Repression and Epithelial to Mesenchymal Transition. *J. Biol. Chem.* **2014**, *289* (2), 930–941.
- (41) Zhou, G.; Dada, L. A.; Wu, M.; Kelly, A.; Trejo, H.; Zhou, Q.; Varga, J.; Sznajder, J. I. Hypoxia-induced alveolar epithelial-mesenchymal transition requires mitochondrial ROS and hypoxia-inducible factor 1. *Am. J. Physiol Lung Cell Mol. Physiol.* **2009**, *297* (6), L1120–L1130.
- (42) Rico-Leo, E. M.; Alvarez-Barrientos, A.; Fernandez-Salguero, P. M. Dioxin Receptor Expression Inhibits Basal and Transforming Growth Factor β-induced Epithelial-to-mesenchymal Transition. *J. Biol. Chem.* **2013**, *288* (11), 7841–7856.
- (43) Maeda, G.; Chiba, T.; Aoba, T.; Imai, K. Epigenetic inactivation of E-cadherin by promoter hypermethylation in oral carcinoma cells. *Odontology* **2007**, *95* (1), 24–29.
- (44) Kim, D. S.; Kim, M. J.; Lee, J. Y.; Kim, Y. Z.; Kim, E. J.; Park, J. Y. Aberrant methylation of E-cadherin and H-cadherin genes in non-small cell lung cancer and its relation to clinicopathologic features. *Cancer* **2007**, *110*, 2785–2792.
- (45) Chen, C. L.; Liu, S. S.; Ip, S. M.; Wong, L. C.; Ng, T. Y.; Ngan, H. Y. E-cadherin expression is silenced by DNA methylation in cervical cancer cell lines and tumours. *Eur. J. Cancer* **2003**, *39* (4), 517–523.
- (46) Damiani, L. A.; Yingling, C. M.; Leng, S.; Romo, P. E.; Nakamura, J.; Belinsky, S. A. Carcinogen-induced gene promoter hypermethylation is mediated by DNMT1 and causal for transformation of immortalized bronchial epithelial cells. *Cancer Res.* **2008**, *68*, 9005–9014.
- (47) Zhang, R. L.; Peng, L. X.; Yang, J. P.; Zheng, L. S.; Xie, P.; Wang, M. Y.; Huang, B. J.; Zhao, H. R.; Bao, Y. X.; Qian, C. N. IL-8 suppresses E-cadherin expression in nasopharyngeal carcinoma cells by enhancing E-cadherin promoter DNA methylation. *Int. J. Oncol.* **2016**, *48* (1), 207–214.
- (48) Lim, S. O.; Gu, J. M.; Kim, M. S.; Kim, H. S.; Park, Y. N.; Park, C. K.; Cho, J. W.; Park, Y. M.; Jung, G. Epigenetic changes induced by reactive oxygen species in hepatocellular carcinoma: Methylation of the E-cadherin promoter. *Gastroenterology* **2008**, *135* (6), 2128–2140.
- (49) Shvedova, A. A.; Kisin, E.; Murray, A. R.; Johnson, V. J.; Gorelik, O.; Areppalli, S.; Hubbs, A. F.; Mercer, R. R.; Keohavong, P.; Sussman, N.; Jin, J.; Yin, J.; Stone, S.; Chen, B. T.; Deye, G.; Maynard, A.; Castranova, V.; Baron, P. A.; Kagan, V. E. Inhalation vs. aspiration of single-walled carbon nanotubes in C57BL/6 mice: inflammation, fibrosis, oxidative stress, and mutagenesis. *Am. J. Physiol Lung Cell Mol. Physiol.* **2008**, *295*, L552–L565.
- (50) Shvedova, A. A.; Kisin, E. R.; Mercer, R.; Murray, A. R.; Johnson, V. J.; Potapovich, A. I.; Tyurina, Y. Y.; Gorelik, O.; Areppalli, S.; Schwegler-Berry, D.; Hubbs, A. F.; Antonini, J.; Evans, D. E.; Ku, B. K.; Ramsey, D.; Maynard, A.; Kagan, V. E.; Castranova, V.; Baron, P. Unusual inflammatory and fibrogenic pulmonary responses to single walled carbon nanotubes in mice. *Am. J. Physiol Lung Cell Mol. Physiol.* **2005**, *289*, L698–L708.
- (51) Cao, L. X.; Geng, H.; Yao, C. T.; Zhao, L.; Duan, P. L.; Xuan, Y. Y.; Li, H. Investigation of chemical compositions of atmospheric fine particles during a wintertime haze episode in Taiyuan City. *China Environ. Sci.* **2014**, *34*, 259–265.